Egyptian Journal of Chemistry

http://ejchem.journals.ekb.eg/

STRUCTURAL INVESTIGATION OF Fe_2O_3–Bi_2O_3–B_2O_3 GLASSES

K. El-Egili * and R. Ghazal

Glass Research Group, Physics Department, Faculty of Science, Mansoura University, Mansoura 35516, Egypt

Abstract

The structure of $x$$Fe_2O_3$·(30-$x$)$Bi_2O_3$·70$B_2O_3$ and $x$$Fe_2O_3$·(50-$x$)$Bi_2O_3$·50$B_2O_3$ glasses (mol%) was investigated by FTIR, XRD and SEM. Increasing Fe_2O_3 content causes decreasing in the fraction N_4 of four coordinated boron atoms of both series. FTIR analyses indicate that Fe_2O_3 tends preferentially to form its former matrix and the majority of BO_4 units are modified by Bi^{3+} ions. XRD patterns confirm that only α-Fe_2O_3 crystalline phase appears in the glasses with $Fe_2O_3 \geq 15$ mol% for the first group and $Fe_2O_3 \geq 25$ mol% for the second one. 50Bi_2O_3–50B_2O_3 glass in the second group has tendency to crystallization when heat treated. SEM shows that spherical particles are separated from the main matrix with different sizes in both glass groups. There is a linear decrease of density in both series with replacing Bi_2O_3 by Fe_2O_3. The molar volume seems to be constant in the first group, whereas it decreases in the second one. Calculated density and molar volume are in a good agreement with the experimental data.

keywords: Fe_2O_3– Bi_2O_3–B_2O_3 glasses; X-ray: SEM; FTIR spectra; Density–structure correlations ;

1. Introduction

Glasses containing Bi_2O_3 well known to have more interest in the field of superconductor materials [1], thermal, mechanical sensors [2] and fast ion conducting glasses [3]. The high polarizability of Bi^{3+} make them suitable for many optical tools [4]. Raman and infrared spectral investigations of B_2O_3–Bi_2O_3 glasses doped with small amount of Fe_2O_3 [5] and CuO [2] indicated that Bi^{3+} cations are incorporated in the glass network as BiO_3 pyramidal and BiO_6 octahedral units for lower content of Bi_2O_3 and as distorted BiO_6 polyhedra for higher content. Infrared spectra of bismuth borate [6] glasses involving 30–60 mol% Bi_2O_3 are characterized with their short-range order structure. Presence of Bi_2O_3 causes a rapid conversion of BO_3 to BO_4 groups. In addition, Bi_2O_3 in the form of BiO_6 octahedral units plays the role of glass former. FTIR studies of $x$$Gd_2O_3$·(100-$x$)[2$Bi_2O_3$·$B_2O_3$] [7] show that the glass structure consists of BiO_6, BO_3 and BO_4 units, but their

proportion depends on Gd^{3+} content in these glasses. In addition, Gd^{3+} play the role of a network modifier while both Bi_2O_3 and B_2O_3 behave as network formers. Previous investigations of V_2O_5–Bi_2O_3–Fe_2O_3 [8] have reported that both V_2O_5 and Bi_2O_3 can play a dual role in the glass network. The existence of several structural units, i.e., VO_5, VO_4, BiO_6, FeO_6 and FeO_4 has been proved. On the other hand, the existence of iron ions in glass matrices in different valence states with different coordinations has its influence on the physical and structural properties [9]. It is reported that the trivalent iron ions can take two different coordination sites, namely tetrahedral or octahedral sites in glasses. Hence, Fe shares in glass matrix as Fe^{2+} and Fe^{3+} and results in various modified structural units [10]. Also it's believed that Fe_2O_3 often plays a dual function at lower concentrations, it acts as a modifier and behaves as a glass former for the higher concentrations depending on the glass matrix. As a consequence, it can imply a proclivity to shape a new glassy phase in certain cases [11, 12]. The present work aims to study the structure of Fe_2O_3–Bi_2O_3–B_2O_3

glasses. The influence of Fe_2O_3 content on the structure and some physical properties of these glasses are investigated by using FTIR spectroscopy, X-ray diffraction (XRD) and Scanning electron microscope (SEM).

2. Experimental

Two glass groups; $xFe_2O_3 \cdot (30-x)Bi_2O_3 \cdot 70B_2O_3$ (labeled as 30BiFeB) and $xFe_2O_3 \cdot (50-x)Bi_2O_3 \cdot 50B_2O_3$ (50BiFeB) were prepared by melting homogeneous mixtures of high purity H_3BO_3, Bi_2O_3 and Fe_2O_3 (with purity not less than 98%). In these groups, Fe_2O_3 could be introduced to the Bi_2O_3–B_2O_3 network up to 20 mol% in 30BiFeB glasses whereas it could be added up to 35 mol% in 50BiFeB glasses. The powdered samples were mixed together in porcelain crucibles in an electric furnace under normal temperature and pressure conditions at temperature ranging between 800 and 1150 °C for 30-40 min., depending on the glass composition. The melt was swirled frequently to ensure the homogeneity. After melting, the refined melt was poured on a steel plates and then pressed with another steel plate to obtain glass disks at room temperature.

KBr pellet technique was used to get the FTIR absorption spectra of the studied glasses. The glassy specimens were grinded in a gate morter then mixed with KBr at ratio 1:100 in weight. A Mattson FTIR spectrometer, with a 2 cm^{-1} resolution, was used to get the spectra in range 400-4000 cm^{-1} at room temperature in average 20 scans are accumulated to form the spectra of each sample. FTIR spectra have been analyzed by deconvolution method.

A cautious deconvolution of the absorption profiles using the peak fit program was used to perform a quantitative analysis for the infrared spectrum. Two-point baseline correction was used to correct IR spectra for dark current noises and history. Many trails have been performed using various band types, but the best match was discovered to be the Gaussian form. The software automatically adjusts the location of each band, as well as its width and strength, based on the minimization of differences between the experimental and simulated spectrum.

Both short and long range orders of the glass matrix have been examined by using a Bruker D8 Advanced power XRD instrument. It is filled with a vantech

super speed position sensitive detector and a Cu-Ka X-ray tube with a gobel mirror. Measurements were made over the range 4° to 70° on 2θ scale using a dwell time of 0.4 s.

SEM model JEOL-JSM-6510 LV, operated at accelerating voltage up to 30 kV was used to follow up the morphological changes and a surface modification of glass samples. Samples were etched at room temperature for (10 min) using HF solution (5%).

Density is calculated by using Archimedes method, with xylene as immersion fluid. At least four samples of each glass was used to determine the density. Density values are precise to ~ ±0.4 g/cm^3. The molar volume was obtained from the relation $Vm = M/D$, where M is the molecular weight of the glass.

3. Result and discussion
3.1 Infrared spectra

Fig. 1 (a, b) shows the infrared spectra (FTIR) of two $xFe_2O_3 \cdot (30-x)Bi_2O_3 \cdot 70B_2O_3$ (30BiFeB) and $xFe_2O_3 \cdot (50-x)Bi_2O_3 \cdot 50B_2O_3$ (50BiFeB) glass groups, respectively. The main vibrational modes of the borate network are observed for all glass compositions which present mainly in two infrared bands ~740–1170 cm^{-1} and ~1170–1600 cm^{-1}. In addition, there are two small absorption bands at 450 and 680 cm^{-1}. In pure B_2O_3 glass, the absorption IR band at ~740–1170 cm^{-1} is referred to B–O bond of BO_4 units [13 ,14]. The second absorption band in the region ~1170–1600 cm^{-1} is due to stretching vibrations in symmetric and asymmetric BO_3 units [13, 15]. The band at 450 cm^{-1} is attributed to the Bi–O bending vibration of BiO_6 structural units for binary Bi_2O_3–B_2O_3 glasses [7]. Further, the absorption band seen at around 680 cm^{-1} is related to bending vibration of B–O–B linkage in the borate network [16]. It is observed also that, the relative area under the band in the region ~740–1170 cm^{-1} decreases whereas that under the band in the region ~1170–1600 cm^{-1} and under the peak at 680 cm^{-1} is increased up on Fe_2O_3 addition. This indicates that the concentration of BO_3 units increases at the expense of BO_4 units. For glasses ≥ 15 mol% Fe_2O_3 in 30FeBiB group and ≥ 25 mol% Fe_2O_3 for 50FeBiB
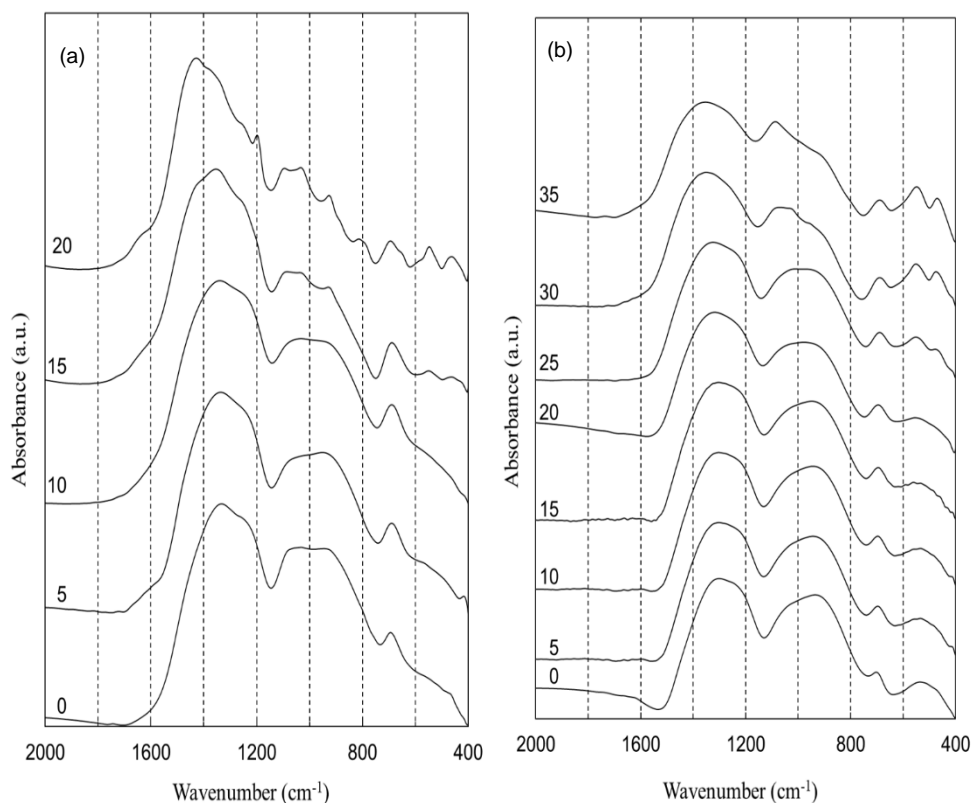
Fig. 1. Infrared spectra of (a) xFe$_2$O$_3$·(30 − x)Bi$_2$O$_3$·70B$_2$O$_3$ (30BiFeB) and (b) xFe$_2$O$_3$·(50–x) Bi$_2$O$_3$·50B$_2$O$_3$ (50BiFeB) glasses. Numbers at the plots refer to Fe$_2$O$_3$ content (mol%).

group, the absorption region 400–600 cm^{-1} shows splitting to two small bands at 470 and 550 cm^{-1}. These bands are related to the vibrations of Fe–O bond in FeO$_6$ and FeO$_4$ structural units, respectively [9]. In addition, the area under these peaks increases with increasing Fe$_2$O$_3$ content. This indicates that, Fe$_2$O$_3$ plays a dual role as network former and modifier [17]. The Bi-O band in this region may masked by the Fe-O bands. Further, there is splitting of the absorption region ~740–1170 cm^{-1} to smaller peaks for glass containing 20 mol% Fe$_2$O$_3$ in 30FeBiB group. Further, the same region for glass containing 35 mol% Fe$_2$O$_3$ in 50FeBiB group becomes two shoulders in the region between 740-1000 cm^{-1} and small peak at 1080 cm^{-1}. Such features reflect some structural changes in these glasses. These changes may be related to the higher tendency of these glasses for crystallization. On the other hand, the center of the absorption region ~1170–1600 cm^{-1} for both glass groups shifts to higher wavenumber. This may be due to the formation of more BO$_3$ units at the expense of BO$_4$ units as will be seen later.

The fraction N_4 of four coordinated boron for the investigated glasses can be obtained by deconvoluting the plots shown in Fig. 1 (a, b). According to the deconvolution method N_4 is calculated as follow (the area associated to BO$_4^-$ units / the total area of BO$_3$ and BO$_4^-$ units). This method was successfully used for some borate [18, 19] and borosilicate [20] glasses to calculate N_4 from the infrared spectra. In addition, it was also used to determine the concentration of the different structural units in tellurite glasses [21]. Fig.
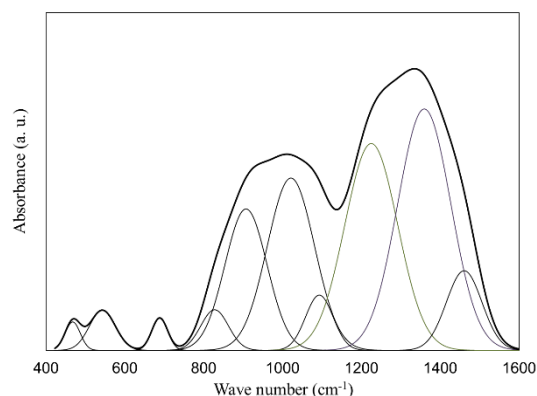

Fig. 2. Deconvolution of the normalized infrared spectrum of the glass 25Fe$_2$O$_3$– 25Bi$_2$O$_3$–50B$_2$O$_3$

_____

2 shows deconvolution of the infrared spectrum of $25Fe_2O_3–25Bi_2O_3$ $50B_2O_3$ glass, as an example.

Figure 3 shows the dependence of N_4 on Fe_2O_3 content in $xFe_2O_3 \cdot (30–x)Bi_2O_3 \cdot 70B_2O_3$ and $xFe_2O_3 \cdot (50–x)Bi_2O_3 \cdot 50B_2O_3$ glass groups. It appears that N_4 for glasses at $x = 0$ agree well with the NMR data given by Bajaj et al. [22]. In addition, N_4 decreases with increasing Fe_2O_3 content for the studied glass groups. The rate of decrease of N_4 for glasses in 30BiFeB group is higher than that of 50BiFeB group.
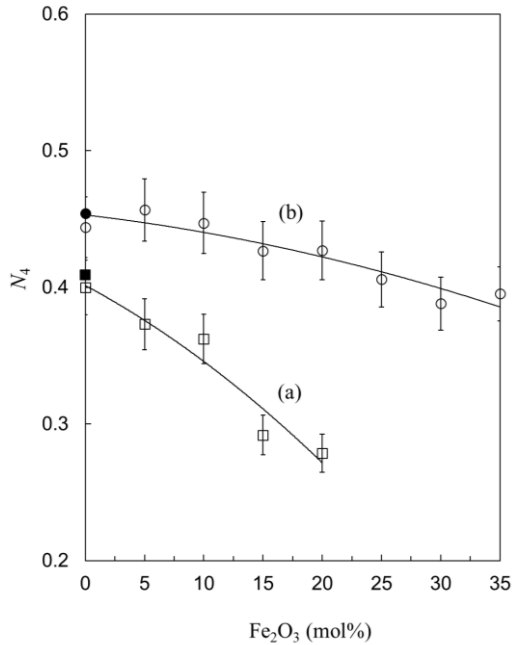

Fig. 3. Fraction N_4 of four-coordinated boron in (a) $xFe_2O_3 \cdot (30 – x)$ $Bi_2O_3 \cdot 70B_2O_3$ (30BiFeB) glasses and (b) $xFe_2O_3 \cdot (50 – x)$ $Bi_2O_3 \cdot 50B_2O_3$ (50BiFeB) glasses. The open symbol refers to experimental data. the error limit is estimated as $\pm$ 5%. The filled symbol for the value $x = 0$ is predicted from NMR data given by Bajaj et al. [22].

In Fig. 3 the equation of the fitting of N_4 for 30BiFeB glass group is

$$N_4 = -9.2809E\text{-}05x^2 – 0.004625676x + 0.401335731 \qquad (1)$$

whereas that for 50BiFeB glass group is

$$N_4 = -2.59089E\text{-}05x^2 – 0.001016559x + 0.452981604 \qquad (2)$$

It is supposed that N_4 represents the consequent modification of borate matrix. Taking in consideration in the case of including more than one type of modifier, each modifier shares for N_4 with specific factor that relies on the modifier content [23, 24]. This can be formulated as

$$N_4 = N_{4(Fe)} + N_{4(Bi)}. \qquad (3)$$

Here, $N_{4(Fe)}$ and $N_{4(Bi)}$ are, respectively, the

participation of Fe_2O_3 and Bi_2O_3 content to N_4 of glass. N_4 can be correlated to the concentration of Fe_2O_3 and Bi_2O_3 by
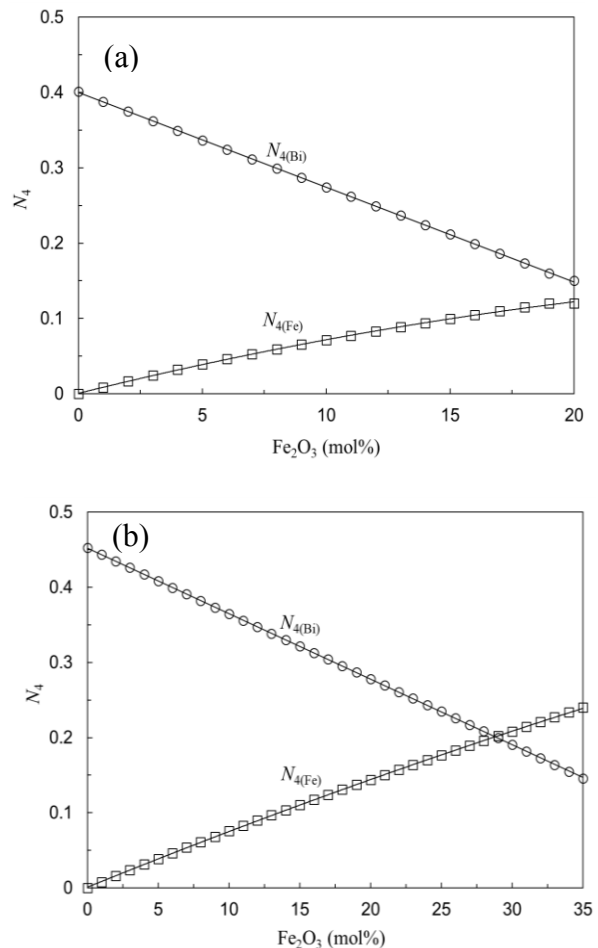
$$N_4 = C_{Fe} f_{Fe} + C_{Bi} f_{Bi} \qquad (4)$$

where C_{Fe} and C_{Bi} are, respectively, the molar fraction of Fe_2O_3 and Bi_2O_3 in glass. While f_{Fe} and f_{Bi} are, respectively, numerical factor that determine how much of Fe_2O_3 and Bi_2O_3 shares to N_4. From Eqs. (3) and (4) it clarifies that

$$N_{4(Fe)} = C_{Fe} f_{Fe} \qquad (5)$$

and

$$N_{4(Bi)} = C_{Bi} f_{Bi}. \qquad (6)$$

N_4 data obtained from Eqs. (1) and (2) can be used to get f_{Fe} and f_{Bi} for the 30BiFeB and 50BiFeB glass

Fig. 4. The dependence of fractions $N_{4(Fe)}$ and $N_{4(Bi)}$ in (a) $xFe_2O_3 \cdot (30 – x)$ $Bi_2O_3 \cdot 70B_2O_3$ (30BiFeB) and (b) $xFe_2O_3 \cdot (50 – x)$ $Bi_2O_3 \cdot 50B_2O_3$ (50BiFeB) glasses with Fe_2O_3 content

groups, and therefore to determine the values of $N_{4(Fe)}$ and $N_{4(Bi)}$. This can be obtained by solving Eq. (4) simultaneously for two N_4 values near to each other and then by substituting in Eqs. (5) and (6). Fig. 4 (a, b) shows that $N_{4(Bi)}$ decreases whereas $N_{4(Fe)}$ increases with increasing Fe_2O_3 content for both glass groups. It is observed that, the rate of decreasing of $N_{4(Bi)}$ is higher than the rate of increasing of $N_{4(Fe)}$ for all glass

groups, which explains the decrease in N_4 (Fig. 3) in spite of the increase in Fe_2O_3 content. In addition, at 20 mol% Fe_2O_3 the values of $N_{4(Fe)}$ and $N_{4(Bi)}$ for 50BiFeB glass group are higher than those for 30BiFeB glass group. This explains the higher rate of decrease of N_4 for glasses in 30BiFeB group (Fig. 3).

From Eqs. (5) and (6) the concentration of various structural units for 30BiFeB and 50BiFeB glass groups can be obtained. The molar fractions of B_2O_3 converted to BO_4 units by Fe_2O_3 ($C_{B4(Fe)}$) and Bi_2O_3 ($C_{B4(Bi)}$) are given, respectively, as

$$C_{B4(Fe)} = N_{4(Fe)} \, C_B \qquad (7)$$

and

$$C_{B4(Bi)} = N_{4(Bi)} \, C_B. \qquad (7a)$$

Here, C_B is the molar fraction of B_2O_3 in the glass group (0.7 for 30BiFeB and 0.5 for 50BiFeB). Therefore, the molar fractions of modifier Fe_2O_3 ($C_{Fe(m)}$) and Bi_2O_3 ($C_{Bi(m)}$) becomes

$$C_{Fe(m)} = C_{4(Fe)}/3 \qquad (8)$$

and

$$C_{Bi(m)} = C_{4(Bi)}/3 \qquad (8a)$$

The factor (1/3) appears because each one molecule of modifier Fe_2O_3 or Bi_2O_3 would alters three B_2O_3 molecules to six BO_4 units. In addition, it is known that Fe_2O_3 and Bi_2O_3 inter the glass structure as network former and modifier [6], [17], [25]. Therefore, the fraction ($C_{Fe(f)}$) of the former Fe_2O_3 can be given as

$$C_{Fe(f)} = C_{Fe} - C_{Fe(m)}. \qquad (9)$$

Similarly, the fraction of the former Bi_2O_3 ($C_{Bi(f)}$) can be given as

$$C_{Bi(f)} = C_{Bi} - C_{Bi(m)} \qquad (10)$$

Finally, the fraction of symmetric BO_3 units (C_{B3s}) of B_2O_3 that remains without being modified can be given as

$$C_{B3s} = C_B - C_{B4(Fe)} - C_{B4(Bi)}. \qquad (11)$$

Fig. 5 (a, b) shows the dependence of the quantities given by Eqs. (7–11) with Fe_2O_3 content for 30BiFeB and 50BiFeB glass groups, respectively. There is a linear increase in $C_{Fe(m)}$ and $C_{Fe(f)}$ while $C_{Bi(m)}$ and $C_{Bi(f)}$ linearly decrease with increasing Fe_2O_3. These changes are expected due to the increase in Fe_2O_3 at the expense of Bi_2O_3. Further, for all glasses, the rate of increase in $C_{Fe(f)}$ is always greater than that of $C_{Fe(m)}$ and the values of $C_{Bi(m)}$ is higher than that of $C_{Fe(m)}$ except the glass contains 35 mol% Fe_2O_3 for 50BiFeB group. This indicates that Fe_2O_3 tends preferentially to form its former matrix rather than modifying the borate network to from BO_4 units and the majority of BO_4 units were formed by Bi^{3+}. It is noticed that, C_{B3s} linearly increases with ~ 1.21 times for 30BiFeB

glasses and ~ 1.15 times for 50BiFeB glasses which is consistence with the increase in the relative area of the envelopes between 1170 cm^{-1} and 1600 cm^{-1} as in Fig. 1 (a, b). This is mainly related to two reasons; the first is the decrease in Bi_2O_3 content in the glass matrix i.e. BO_4 units decrease, and the second is the weak capability of Fe_2O_3 to compose BO_4 units i.e. BO_3 units increase. Similar behavior was observed in Sb_2O_3–PbO–B_2O_3 glasses [18].
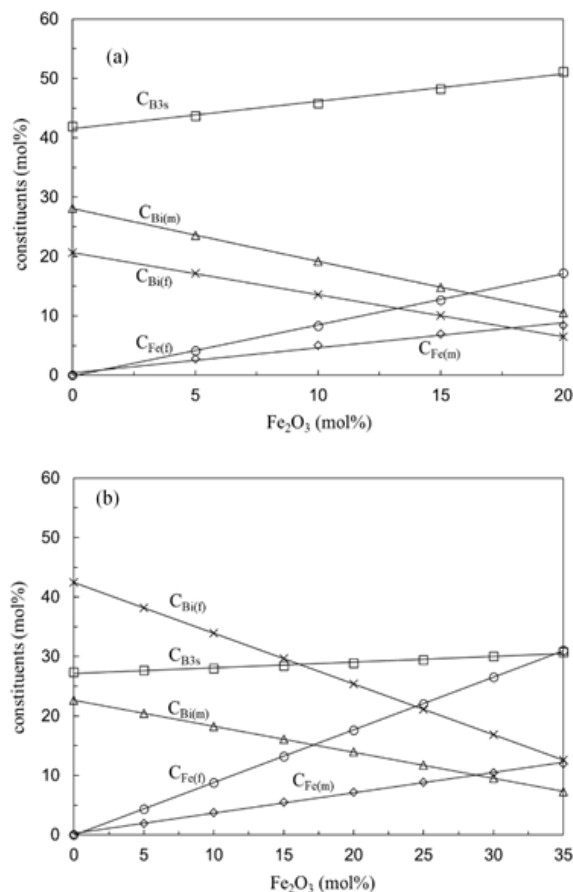

Fig. 5. The dependence of $C_{Fe(m)}$, $C_{Fe(f)}$, $C_{Bi(m)}$, $C_{Bi(f)}$ and C_{B3s} in (a) $xFe_2O_3 \cdot (30-x)$ $Bi_2O_3 \cdot 70B_2O_3$ (30BiFeB) and (b) $xFe_2O_3 \cdot (50-x)$ $Bi_2O_3 \cdot 50B_2O_3$ (50BiFeB) glasses on Fe_2O_3 content. $C_{Fe(m)}$ and $C_{Fe(f)}$ are, respectively, the fractions of modifier and former Fe_2O_3. $C_{Bi(m)}$ and $C_{Bi(f)}$ are, respectively, the fractions of modifier and former Bi_2O_3. C_{B3s} is the fraction of B_2O_3 that forms symmetric BO_3 units. Lines are drawn as guides to the eyes.

From a numerical overview, at 20 mol% Fe_2O_3 (Fig. 5a), the glass is composed ~ 51 mol% B_2O_3 as sym. BO_3 units, ~ 10.5 mol% B_2O_3 as BO_4 units modulated by Bi^{3+}, ~ 8.4 mol% B_2O_3 as BO_4 units modulated by Fe^{3+} and former units of Fe_2O_3 (~ 17.2 mol%) and Bi_2O_3 (~ 6.5 mol%). This means that the majority of such glass is consist of a borate rich phase ~ 70 mol% as host matrix and just ~ 23.7 mol% as former units of Fe_2O_3 and Bi_2O_3. Whereas, at 35 mol%

Fe_2O_3 (Fig. 5b) the glass is composed ~ 30.7 mol% B_2O_3 as sym. BO_3 units, ~ 7.28 mol% B_2O_3 as BO_4 units modified by Bi^{3+}, ~ 12 mol% B_2O_3 as BO_4 units modified by Fe^{3+} and former units of Fe_2O_3 (~ 31 mol%) and Bi_2O_3 (~ 12.57 mol%). This means that such glass is composed a higher ratio of former units ~ 43.57 mol% and the borate phase ~ 50 mol% as host matrix.

Fig. 6 (a, b) shows the dependence in density (D) and molar volume (V_m) with Fe_2O_3 content for 30BiFeB and 50BiFeB glass groups, respectively.
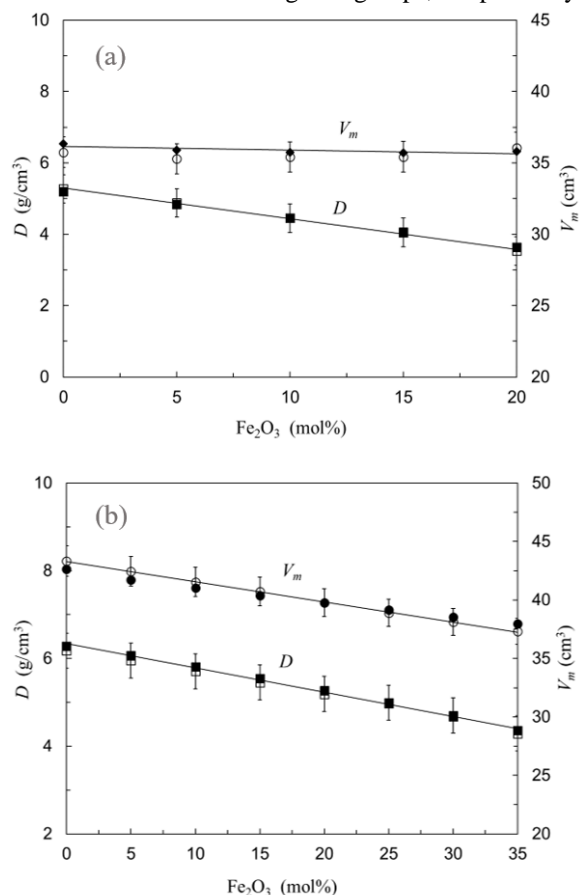

Fig. 6. Change with composition of D and V_m of (a) $xFe_2O_3 \cdot (30-x)$ $Bi_2O_3 \cdot 70B_2O_3$ (30BiFeB) and (b) $xFe_2O_3 \cdot (50 - x)$ $Bi_2O_3 \cdot 50B_2O_3$ (50BiFeB) glasses. Open and closed symbols, respectively, represent experimental and calculated results.

Figure 6a shows a linear decrease in D whereas V_m seems to be constant, while both D and V_m linearly decrease in Fig. 6b with increasing Fe_2O_3 content. These changes reveal that both of Fe_2O_3 and Bi_2O_3 contribute to D and V_m with constant rates. The decrease in D is expected because the relative molecular mass of Fe_2O_3 (159.69 g/mol) is much smaller than that of Bi_2O_3 (465.96 g/mol). In this case, one would expect an increase in V_m because D and V_m mostly change inversely to each other. Therefore, the

changes in D and V_m indicate that both of them is correlated with the relative change in the structural units in the glass matrix due to introduction of Fe_2O_3 at the expense of Bi_2O_3 rather than the big deference between their relative molecular masses.

It is concluded [18], [24], [26] that the glass is composed of various structural units that form its network and the variation in D and V_m, must be interpreted in the light of the change in glass composition. The decrease in D Fig. 6 (a, b) indicates that the structural units associated with Fe_2O_3 are less dense and have smaller volume than those corresponding to Bi_2O_3.

By using Eqs. (7)–(11) one can interprets the factors influencing the D based on the structural units in the glass. It is known that, the density is considered as the sum of masses of structural units divided by the sum of their volumes. Therefore, the density of a glass can be expressed as

$$D = \frac{\sum_u n_u M_u}{\sum_u n_u V_u} \qquad (12)$$

Where, n_u symbolizes the content of structural unit u (number per mole of glass). M_u and V_u point, respectively, to the mass and volume of unit. M_u represents the sum of masses of atoms in the unit. As well as, V_u represents the resultant volume of atoms and its surrounding space (free volume) in the unit in the glass matrix. As previously shown, the structure of the studied glasses consists of $BO_{4(Fe)}$, $BO_{4(Bi)}$, $Fe_{(f)}$, $Bi_{(f)}$ and the symmetric BO_3 units. Therefore, Eq. (12) can then be rewritten as

$D = (n_{4(Fe)}M_{4(Fe)} + n_{4(Bi)}M_{4(Bi)} + n_{Fe(f)}M_{Fe(f)} + n_{Bi(f)}M_{Bi(f)} + n_3M_{3s}) / (n_{4(Fe)}V_{4(Fe)} + n_{4(Bi)}V_{4(Bi)} + n_{Fe(f)}V_{Fe(f)} + n_{Bi(f)}V_{Bi(f)} + n_3V_{3s})$. (13)

Here, $n_{4(Fe)}$, $n_{4(Bi)}$, $n_{Fe(f)}$, $n_{Bi(f)}$ and n_3 refer, respectively, to the number per mole of glass of the units $BO_{4(Fe)}$, $BO_{4(Bi)}$, $Fe_{(f)}$, $Bi_{(f)}$ and BO_{3s}. Masses and volumes in Eq. (13) are pointed to the corresponding units.

According to these hypotheses, $M_{Fe(f)}$ (in Eq. 13) is considered as the mass of former FeO_4 unit (mass of Fe + 2O), $M_{Bi(f)}$ is the mass of former BiO_3 unit (mass of Bi + 1.5O) and M_3 is the mass of BO_3 unit (B + 1.5O). In addition, each BO^-_4 unit associated with a negative charge that could be neutralized by one of the three positive charges of Fe^{3+} or Bi^{3+} ion. Therefore, $M_{4(Fe)}$ is the mass of (B + 2O + Fe/3) and $M_{4(Bi)}$ represents the mass of (B + 2O + Bi/3). The
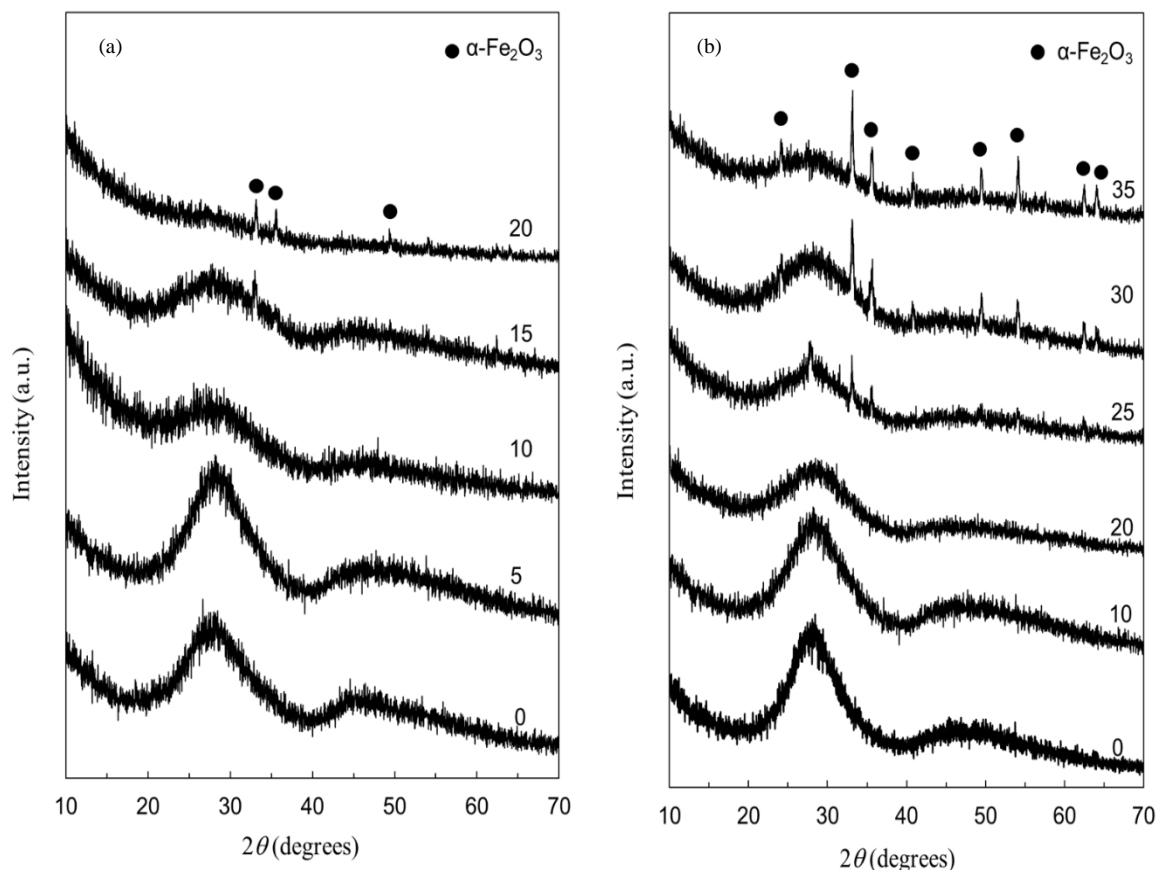
Fig. 7. XRD patterns of (a) xFe$_2$O$_3$·(30–x) Bi$_2$O$_3$·70B$_2$O$_3$ (30BiFeB) and (b) xFe$_2$O$_3$·(50–x) Bi$_2$O$_3$·50B$_2$O$_3$ (50BiFeB) glasses. Numbers at the plots refer to Fe$_2$O$_3$ content (mol%).

concentration of structural units $n_{4(Fe)}$, $n_{4(Bi)}$, $n_{Fe(f)}$, $n_{Bi(f)}$ and n_3 in Eq. (13) can be got from Eqs. (7–11), respectively, as

$$n_{4(Fe)} = 2N_A\, C_{B4(Fe)}, \tag{14}$$
$$n_{4(Bi)} = 2N_A C_{B4(Bi)}, \tag{15}$$
$$n_{Fe(f)} = 2N_A C_{Fe(f)}, \tag{16}$$
$$n_{Bi(f)} = 2N_A C_{Bi(f)} \tag{17}$$

and

$$n_3 = 2N_A C_{B3s}. \tag{18}$$

The factor 2 arises because each B$_2$O$_3$ molecule produces two BO$_3$ or two BO$_4$ units. Also, each Fe$_2$O$_3$ or Bi$_2$O$_3$ molecule produces two FeO$_4$ units or two BiO$_3$ as former units and N_A is Avogadro's number. the density can be calculated from Eq. (13) if the volumes of the structural units were well defined. The volumes of $V_{4(Bi)}$ and $V_{Bi(f)}$ are calculated from binary xBi$_2$O$_3$–$(1-x)$B$_2$O$_3$ [27] glasses, in addition to that of V_{3s} from vitreous B$_2$O$_3$ [19]. These volumes can be used as a guide to solve Eq.13 to get $V_{4(Fe)}$ and $V_{Fe(f)}$ for iron oxide. These are $V_{4(Bi)} = 2.29 \times 10^{-23}$ cm^3 and $V_{Bi(f)}$ $= 5.05 \times 10^{-23}$ cm^3 and $V_{3s} = 3.14 \times 10^{-23}$ cm^3. Then, trials can be done to find the values of $V_{4(Fe)}$ and $V_{Fe(f)}$ that leads to agreement between the calculated and experimental densities. The values obtained are $V_{4(Fe)}$ $= 1.681 \times 10^{-23}$ cm^3 and $V_{Fe(f)} = 3.823 \times 10^{-23}$ cm^3. Fig. 6 (a, b) shows good agreement between the calculated and experimental densities. It is clear that, the volume of the structural unit including Bi^{3+} ($V_{4(Bi)}$) is higher than that including Fe^{3+} ($V_{4(Fe)}$) because of the greater size of Bi^{3+} ion with respect to Fe^{3+}.

According to Eq. (13), V_m can be given by:

$$V_m = n_{4(Fe)}V_{4(Fe)} + n_{4(Bi)}V_{4(Bi)} + n_{Fe(f)}V_{Fe(f)} + n_{Bi(f)}V_{Bi(f)} + n_3 V_{3s}. \tag{19}$$

Good agreement between calculated and experimental V_m data Fig. 6 (a, b) could be achieved by using the previous volumes in Eq. (19). This harmony of D and V_m data is a proof of validity of the presented view on the structure of Fe$_2$O$_3$–Bi$_2$O$_3$–B$_2$O$_3$ glasses.

3.2. X-ray and scanning electron microscopy

Fig. 7 (a, b) shows the X-ray diffraction (XRD) pattern of 30BiFeB and 50BiFeB glass groups, respectively. The features of all spectra are typical for heavy metal oxides specially Bi$_2$O$_3$ glasses. Up to 10 mol% Fe$_2$O$_3$ for 30BiFeB group and 20 mol% Fe$_2$O$_3$ for 50BiFeB group, the XRD patterns show no sharp

peaks, only broad diffraction humps centered at about $2\theta = 28.2°$ and $47.45°$ confirming the amorphous nature of glass samples [28]. However, the existence of broad humps indicate also that some phases are not fully grown and might be nano-crystalline phases or clusters formation embedded in the glass matrix [29, 30]. Due to the limited resolution of normal XRD technique, the presence of a small amount of crystallite cannot be excluded. Especially, if the amount of the crystallite or its sizes is very small [31].

On the other hand, it is observed that the broadness of the humps increases whereas their intensities decreases with increasing Fe_2O_3 content until seems to disappear at 20 mol% Fe_2O_3 for 30BiFeB group (Fig. 7a). These changes may be consistent with the decrease in Bi_2O_3 content in the glasses. Beside the broad humps, sharp peaks start to appear for glass containing $\geq$ 15 mol% Fe_2O_3 for 30BiFeB group and $\geq$ 25 mol% Fe_2O_3 for 50BiFeB group at $2\theta = 24.1$, 33.1, 35.6, 40.6, 49.6, 54.1, 62.5 and 63.9° which could be indexed to lattice planes (012), (104), (110), (113), (024), (116), (214) and (300) respectively. These peaks correspond to α-Fe_2O_3 crystalline phase (PDF # 890597) precipitated in Bi_2O_3−B_2O_3 network [32]. The number of sharp peaks and their intensities increases with increasing Fe_2O_3 content. This indicates that the degree of crystallinity increases as the content of Fe_2O_3 increases. Further, some of sharp peaks are superimposed on the broad humps. This means that the glass structure contains mixture of the amorphous phase of Bi_2O_3 and crystalline α-Fe_2O_3 phase. According to Sherrer's equation [33], the average crystalline size of α-Fe_2O_3 phase is ~ 20 nm.

Fig. 8 shows the X–ray patterns of $30Bi_2O_3$–$70B_2O_3$ and $50Bi_2O_3$–$50B_2O_3$ glasses heat treated at 500°C for 4h. It is observed that, the glass $30Bi_2O_3$–$70B_2O_3$ is not affected with heat treatment. On the other hand, it has been noticed that by heat-treatment a Strong tendency of crystallization for $50Bi_2O_3$–$50B_2O_3$ glass. It shows a broad hump with three sharp peaks at $2\theta = 23.13$, 28.55 and 47.97 which could be indexed to lattice planes (110), (111) and (220) respectively. These peaks are related to α-Bi_2O_3 crystalline phase (PDF # 762478). It is clear that, the main peak superimposed on the broad hump indicates the glass structure contains mixture of amorphous and crystalline phases. Moreover, this confirms that the presence of broad humps in Fig.7 (a, b) reflects some microstructural changes (partial phase separation) of

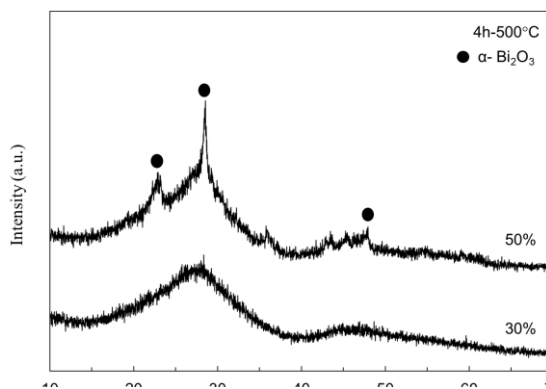small crystallite sizes in bismuth borate matrix [29], [34], [35].

Fig. 8. XRD pattern of heat treated $30Bi_2O_3$–$70B_2O_3$ and $50Bi_2O_3$–$50B_2O_3$ glasses. Heat treatment was performed at 500 °C for 4h.

From the above analyses of the IR data, at 0 mol% Fe_2O_3 in 30BiFeB group (Fig. 5a) the concentration of Bi_2O_3 as former units is ~ 20.64 mol% and that of symmetric BO_3 units is ~ 42 mol% whereas at the same composition in 50BiFeB group (Fig. 5b) the concentrations are ~ 42.45 mol% and ~ 27.35 mol%, respectively. Therefore, it can be deduced that the high concentration of former Bi_2O_3 units and the low concentration of symmetric BO_3 units in 50BiFeB group compared with those in 30BiFeB group are the main reason to form crystalline phase of α-Bi_2O_3 under heat treatment effect (Fig. 8).

The surface morphology has been investigated by scanning electron microscopy (SEM). Fig. 9a shows the micrograph of etched $30Bi_2O_3$–$70B_2O_3$ glass. It is clear that, many isolated spherical particles with different sizes are distributed within a homogeneous glassy phase (the dark background), which indicates the glass structure is not fully amorphous. The big particles (like stone) seem to be formed by collecting small ones. The number of these particles and their sizes increase for etched $50Bi_2O_3$–$50B_2O_3$ glass in the form of clusters of different size between 0.25 μm and 1 μm as shown in Fig. 9b. It can be assumed that the spherical particles in Fig. 9 (a, b) are formed mainly from amorphous Bi_2O_3 which may contain small crystallites of α-Bi_2O_3 phase. On the other hand, the glassy phase (dark background) is assumed to be borate rich phase which consists of symmetric BO_3 and modified BO_4 units. the micrograph of the surface of $20Fe_2O_3$–$10Bi_2O_3$–$70B_2O_3$ glass sample is shown in Fig. 9c. Spherical black droplets of size up to 3 μm separately

(a)

(b)

(c)

(d)

(e)
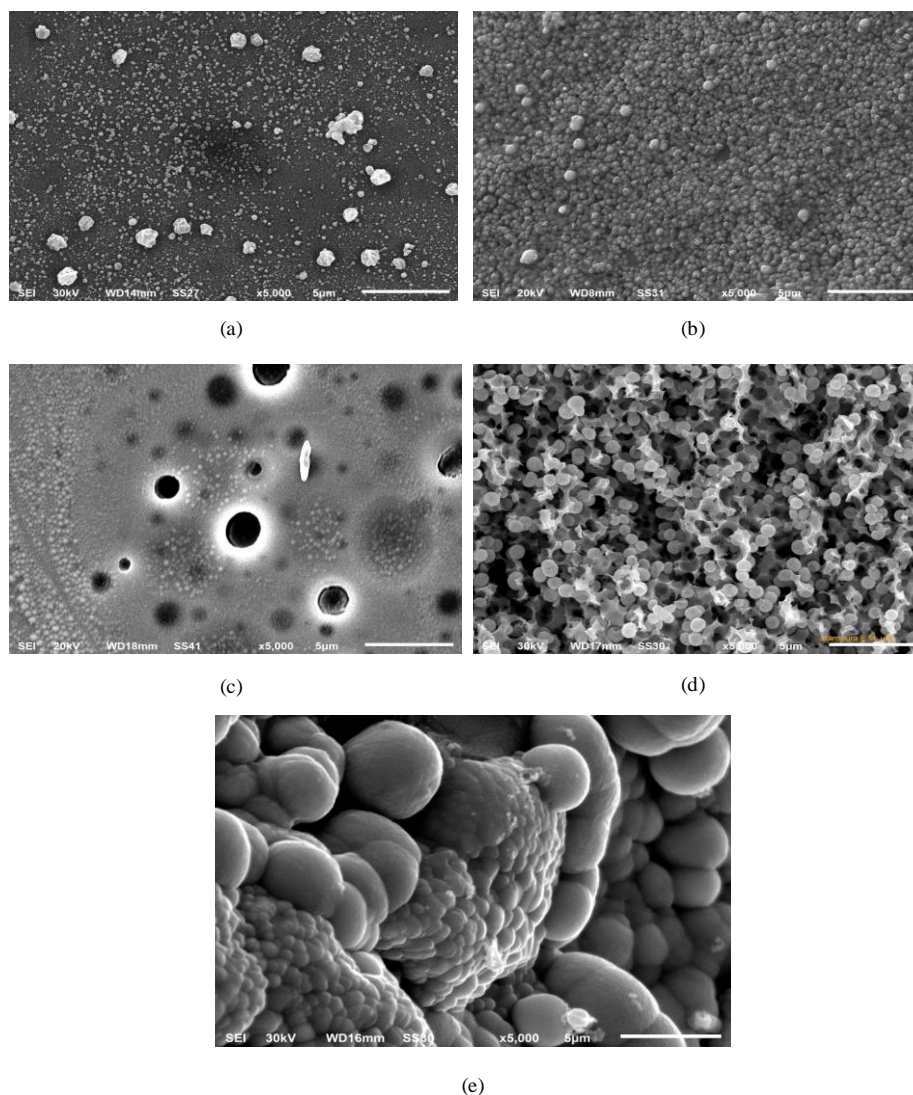
Fig. 9. SEM micrographs of (a) etched $30Bi_2O_3$–$70B_2O_3$ glass, (b) etched $50Bi_2O_3$–$50B_2O_3$ glass, (c) the surface of $20Fe_2O_3$–$10Bi_2O_3$–$70B_2O_3$ glass, (d) etched $20Fe_2O_3·10Bi_2O_3·70B_2O_3$ glass and (e) etched $35Fe_2O_3$–$15Bi_2O_3$–$50B_2O_3$ glass.

distributed and surrounded with white fine particles on the entire glass surface. In the light of X-ray information, the spherical black droplets might be α-Fe_2O_3 phase and the white fine particles may be small crystallites of α-Bi_2O_3. The micrograph of etched $20Fe_2O_3·10Bi_2O_3·70B_2O_3$ glass (Fig. 9d) shows spherical particles are separated from main matrix with size of ~ 0.5 μm. The micrograph of etched $35Fe_2O_3$–$15Bi_2O_3$–$50B_2O_3$ glass shows agglomerates from condensed spherical particles of greater size as shown in Fig. 9e. It can then be assumed that the agglomerates appearing in Fig. 9e are formed of symmetric BO_3 units, modified BO_4 units and vitreous former Bi_2O_3 units.

4. Conclusion

XRD, FTIR and SEM have been used to investigate the structure of $xFe_2O_3·(30-x)Bi_2O_3·70B_2O_3$ and $xFe_2O_3·(50-x)Bi_2O_3·50B_2O_3$ glass groups. FTIR analyses indicate that the majority of BO_4 units modified by Bi^{3+} and Fe_2O_3 tends preferentially to form its former matrix. There is a linear reduction in the portion (N_4) of four coordinated boron atoms and density with rising Fe_2O_3 content. In the first group the molar volume seems to be constant, whereas it decreases in the second one. Calculated density and molar volume are concurrent with the experimental data. XRD exhibit sharp peaks corresponding to α-Fe_2O_3 crystalline phase for high content of Fe_2O_3 and the degree of crystallinity increases with increasing

_____

Fe$_2$O$_3$ content. SEM shows agglomerates consists of vitreous former Bi$_2$O$_3$ units.

4. Conflicts of interest

"There are no conflicts to declare".

5. References

[1] T. Maeder*, 'Review of Bi2O3 based glasses for electronics and related applications', *Int. Mater. Rev.*, vol. 58, no. 1, pp. 3–40, 2013.

[2] L. Baia, R. Stefan, W. Kiefer, J. Popp, and S. Simon, 'Structural investigations of copper doped B2O3–Bi2O3 glasses with high bismuth oxide content', *J. Non. Cryst. Solids*, vol. 303, no. 3, pp. 379–386, 2002.

[3] A. Pan and A. Ghosh, 'Correlation of relaxation dynamics and conductivity spectra with cation constriction in ion-conducting glasses', *Phys. Rev. B*, vol. 66, no. 1, p. 12301, 2002.

[4] M. M. Gomaa, S. Ibrahim, and H. Darwish, 'Effect of SiO 2/B 2 O 3 replacements on the structure, physicochemical and electrical properties of Bi 2 O 3-containing glasses', *Silicon*, vol. 7, no. 1, pp. 55–63, 2015.

[5] L. Baia, D. Maniu, T. Iliescu, S. Simon, S. Schlucker, and W. Kiefer, 'Spectroscopic studies of iron doped B~ 2O~ 3-Bi~ 2O~ 3 glasses', *Asian J. Phys.*, vol. 9, no. 1, pp. 51–58, 2000.

[6] Y. Cheng, H. Xiao, W. Guo, and W. Guo, 'Structure and crystallization kinetics of Bi2O3–B2O3 glasses', *Thermochim. Acta*, vol. 444, no. 2, pp. 173–178, 2006.

[7] P. Pascuta and E. Culea, 'FTIR spectroscopic study of some bismuth germanate glasses containing gadolinium ions', *Mater. Lett.*, vol. 62, no. 25, pp. 4127–4129, 2008.

[8] R. Iordanova, Y. Dimitriev, V. Dimitrov, S. Kassabov, and D. Klissurski, 'Glass formation and structure in the V2O5☐ Bi2O3☐ Fe2O3 glasses', *J. Non. Cryst. Solids*, vol. 204, no. 2, pp. 141–150, 1996.

[9] M. Shapaan and F. M. Ebrahim, 'Structural and electric–dielectric properties of B2O3–Bi2O3–Fe2O3 oxide glasses', *Phys. B Condens. Matter*, vol. 405, no. 16, pp. 3217–3222, 2010.

[10] G. Srinivasarao and N. Veeraiah, 'The role of iron ions on the structure and certain physical properties of PbO–As2O3 glasses', *J. Phys. Chem. Solids*, vol. 63, no. 4, pp. 705–717, 2002.

[11] I. Ardelean, R. Lungu, and P. Păşcuţă, 'Structural changes induced by Fe 2 O 3 addition in strontium-borate glass matrix', *J. Mater. Sci. Mater. Electron.*, vol. 18, no. 8, pp. 837–841, 2007.

[12] F. A. Moustafa, A. M. Fayad, F. M. Ezz-Eldin, and I. El-Kashif, 'Effect of gamma radiation on ultraviolet, visible and infrared studies of NiO, Cr2O3 and Fe2O3-doped alkali borate glasses', *J. Non. Cryst. Solids*, vol. 376, pp. 18–25, 2013, doi: https://doi.org/10.1016/j.jnoncrysol.2013.04.052.

[13] I. Ardelean, S. Cora, and D. Rusu, 'EPR and FT-IR spectroscopic studies of Bi2O3–B2O3–CuO glasses', *Phys. B Condens. Matter*, vol. 403, no. 19–20, pp. 3682–3685, 2008.

[14] H. Doweidar, K. El-Egili, G. El-Damrawi, and R. M. Ramadan, 'Sites distribution and properties of Al2O3–PbO–B2O3 glasses', *Phys. Chem. Glas. J. Glas. Sci. Technol. Part B*, vol. 49, no. 5, pp. 271–277, 2008.

[15] H. Doweidar and Y. B. Saddeek, 'FTIR and ultrasonic investigations on modified bismuth borate glasses', *J. Non. Cryst. Solids*, vol. 355, no. 6, pp. 348–354, 2009.

[16] E. I. Kamitsos, 'Infrared studies of borate glasses', *Phys. Chem. Glas.*, vol. 44, no. 2, pp. 79–87, 2003.

[17] Y. M. Moustafa, K. El-Egili, H. Doweidar, and I. Abbas, 'Structure and electric conduction of Fe2O3–P2O5 glasses', *Phys. B Condens. Matter*, vol. 353, no. 1–2, pp. 82–91, 2004.

[18] H. Doweidar, K. El-Egili, R. Ramadan, and M. Al-Zaibani, 'Structural investigation and properties of Sb2O3–PbO–B2O3 glasses', *J. Non. Cryst. Solids*, vol. 497, pp. 93–101, 2018.

[19] K. El-Egili, H. Doweidar, R. Ramadan, and A. Altawaf, 'Role of F− ions in the structure and properties of BaF2B2O3 glasses', *J. Non. Cryst. Solids*, vol. 449, pp. 83–93, 2016.

[20] K. El-Egili, 'Infrared studies of Na2O–B2O3–SiO2 and Al2O3–Na2O–B2O3–SiO2 glasses', *Phys. B Condens. Matter*, vol. 325, pp. 340–348, 2003.

[21] E. F. El Agammy, H. Doweidar, K. El-Egili, and R. Ramadan, 'Structure of PbF2–TeO2

_____

glasses and glass-ceramics', *J. Mater. Res. Technol.*, 2020.

[22] A. Bajaj *et al.*, 'Structural investigation of bismuth borate glasses and crystalline phases', *J. Non. Cryst. Solids*, vol. 355, no. 1, pp. 45–53, 2009.

[23] H. Doweidar, K. El-Egili, R. Ramadan, and M. Al-Zaibani, 'Structural units distribution, phase separation and properties of PbO–TiO2–B2O3 glasses', *J. Non. Cryst. Solids*, vol. 466, pp. 37–44, 2017.

[24] H. Doweidar, G. El-Damrawi, E. Mansour, and R. E. Fetouh, 'Structural role of MgO and PbO in MgO–PbO–B2O3 glasses as revealed by FTIR; a new approach', *J. Non. Cryst. Solids*, vol. 358, no. 5, pp. 941–946, 2012.

[25] E. R. Shaaban, M. Shapaan, and Y. B. Saddeek, 'Structural and thermal stability criteria of Bi2O3–B2O3 glasses', *J. Phys. Condens. Matter*, vol. 20, no. 15, p. 155108, 2008.

[26] H. Doweidar, 'Density and molar volume of Li2O–SiO2 glasses in relation to their microstructure', *Phys. Chem. Glas.*, vol. 39, no. 5, pp. 286–289, 1998.

[27] K. El-Egili and R. Ghazal, 'Structural-properties correlation and conductivity of Bi2O3–B2O3 glasses', *work in progress*.

[28] A. Madheshiya, C. Gautam, and S. Kumar, 'Synthesis, structural and X-ray absorption spectroscopy of (PbxBi1-x). TiO3 borosilicate glass and glass ceramics', *J. Asian Ceram. Soc.*, vol. 5, no. 3, pp. 276–283, 2017.

[29] S. Singh and K. Singh, 'Effect of in-situ reduction of Fe3+ on physical, structural and optical properties of calcium sodium silicate glasses and glass ceramics', *J. Non. Cryst. Solids*, vol. 386, pp. 100–104, 2014.

[30] Z. Y. Yao *et al.*, 'Structure and mechanical properties of copper–lead and copper–zinc borate glasses', *J. Non. Cryst. Solids*, vol. 435, pp. 55–68, 2016.

[31] L. Liu, K. C. Chan, and G. K. H. Pang, 'High-resolution TEM study of the microstructure of Zr65Ni10Cu7. 5Al7. 5Ag10 bulk metallic glass', *J. Cryst. Growth*, vol. 265, no. 3–4, pp. 642–649, 2004.

[32] H. Akamatsu, K. Tanaka, K. Fujita, and S. Murai, 'Magnetic phase transitions in Fe2O3–Bi2O3–B2O3 glasses', *J. Phys. Condens. Matter*, vol. 20, no. 23, p. 235216, 2008.

[33] A. L. Patterson, 'The Scherrer formula for X-ray particle size determination', *Phys. Rev.*, vol. 56, no. 10, p. 978, 1939.

[34] A. K. Singh, K. Singh, and N. S. Saxena, 'Effect of annealing on structures and effective thermal conductivity of Se90 In10-chalcogenide glass', *J. Ovonic Res.*, vol. 4, pp. 107–111, 2008.

[35] M. Thomas, *Supplementary cementing materials in concrete*. CRC press, 2013.